Preprints of the 21st IFAC World Congress (Virtual)
Berlin, Germany, July 12-17, 2020

Optimal control of plate motion and camber in a reversing rolling mill ⋆

C. Pietschnig * **A. Ettl** * **U. Knechtelsdorfer** * **A. Steinboeck** *
A. Kugi *,**

* *Christian Doppler Laboratory for Model-Based Process Control in the Steel Industry, Automation and Control Institute (ACIN), TU Wien, Vienna, Austria (e-mail: {pietschnig,ettl,kugi}@acin.tuwien.ac.at)*
** *Automation and Control Institute (ACIN), TU Wien, Vienna, Austria (e-mail: steinboeck@acin.tuwien.ac.at)*

Abstract: In plate rolling, reversing roughing mills are commonly used as a first processing step after casting. They are typically equipped with edger rolls for width reduction. During a rolling pass, lateral asymmetries like temperature gradients or thickness inhomogeneities can cause two major problems. The plate may rotate in the rolling gap and thus move in lateral direction. Another problem is that the plate may leave the mill stand with a cambered shape. In the worst case, these problems entail collisions with the mill stand or other equipment along the roller table. It is an essential control task to avoid such problems. In general, the exit thickness profile and the motion of the plate are controlled by adjusting the roll gap height. The latter has also an influence on the contour shape but, for active control of the plate width and contour shape, the use of edger rolls is more common. This is especially true if the roll gap adjustment is self-retaining, meaning that it cannot be adjusted during a rolling pass. In this work, such a roughing mill and its edger rolls are considered. A mathematical model for the motion and the camber of the plate is derived. Based on this model, a linear quadratic regulator (LQR) for both the plate motion and the resulting camber is developed. It uses the lateral forces of the edgers as control inputs. In a cascaded control structure, these forces are regulated by a subordinate admittance controller. The developed control system is validated in simulation studies.

Keywords: Heavy-plate hot rolling, roughing mill with edger rolls, steel industry, model-based control, camber control, optimal control, Riccati equation

1. INTRODUCTION

Roughing mills are typically used in the production of flat steel products downstream of the casting process and upstream of the (tandem) finishing mill. A typical reversing roughing mill equipped with edger rolls is outlined in Fig. 1. In such roughing mills, the thickness of the plate is reduced in several (reversing) passes. The width of the plates increases due to spreading and can be reduced by the edger rolls. If the edger rolls are located upstream (downstream) of the mill stand, they may be used in forward (reverse) rolling passes only. In this paper, forward (reverse) rolling passes are assigned odd numbers, i. e., 1, 3, 5, ... (even numbers, i. e., 2, 4, 6, ...). In the best case, a straight rectangular-shaped plate without camber and thickness inhomogeneities is produced by the roughing process.

Some mathematical models of the lateral plate motion and stability analyses are reported in the literature. Most publications address tandem finishing mills (Ishikawa et al., 1988; Tarnopolskaya et al., 2005; Gates and Tarnopolskaya, 2008; Lee and Choi, 2014). A roughing mill is considered in (Ettl et al., 2018), where a model of the lateral plate motion is developed and utilized to examine how local asymmetric forces on the entry and exit side of the rolling gap affect the stability of the plate motion.

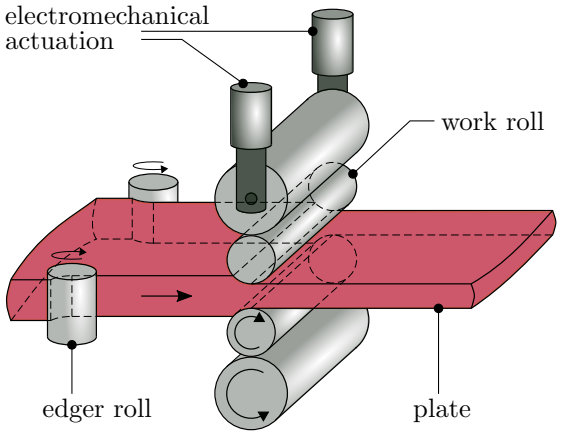

Fig. 1. Reversing roughing mill: forward pass with active edger rolls (Ettl et al., 2018).

Models of the evolution of the plate contour are reviewed in (Steinboeck et al., 2017). Model-based control concepts for camber reduction are given in (Tanaka et al., 1987;

⋆ The financial support by the Christian Doppler Research Association, the Austrian Federal Ministry for Digital and Economic Affairs, the National Foundation for Research, Technology and Development, and voestalpine Stahl GmbH is gratefully acknowledged.

Cuzzola and Dieta, 2003; Schausberger et al., 2016a, 2018). In these works, the roll gap height is adjusted during the rolling pass to minimize the camber of the outgoing plate.

In (Kurz et al., 2015; Kainz et al., 2016), finite element analyses of the camber evolution are reported. The main focus of these works is how camber can be reduced by applying lateral forces to the plate. These papers describe neither the lateral motion of the plate nor a suitable control concept for both, the plate motion and the camber.

There has been also some research on contour detection by camera systems (Yang et al., 2008). In (Schausberger et al., 2015, 2016b), for example, the contour shape and the motion of the plate are estimated with an optimization-based algorithm that uses a kinematic model of the plate.

In this paper, a reversing roughing mill is considered where the roll gap height cannot be adjusted during the rolling pass because of self-retaining electromechanical actuators. In this case, the only control inputs are the lateral forces applied by the edger rolls. The focus of this work are roughing mills, where the product thickness is still high enough to prevent buckling of the product as a consequence of asymmetric edger forces. From Ettl et al. (2018) it is known that edger rolls on the entry side of the roll gap have a stabilizing influence on the plate motion. To perform a safe plate motion during the rolling pass (even if edger rolls are located at the exit side of the roll gap) and to minimize the camber of the outgoing product, a linear quadratic regulator (LQR) is used in the outer loop of a cascade control structure. In the inner loop, an admittance controller positions the edger rolls so that the desired edger forces are realized. The design of the control system as well as its closed-loop performance are investigated for three different scenarios. In the first scenario, the edger rolls are located on the entry side of the roll gap, in the second scenario on the exit side, and the third scenario considers edger rolls on both sides of the roll gap.

In Section 2, a mathematical model of the plate motion and the resulting camber is derived. Section 3 deals with the design of an admittance controller and an LQR in the outer loop. Simulation studies are conducted in Section 4. Section 5 summarizes the outcomes of the paper and gives a short outlook.

2. MATHEMATICAL MODEL

This section describes a mathematical model of the plate motion (Section 2.1) and the evolution of the camber (Section 2.2) during the rolling pass. The outputs of the model are the curvature and the lateral displacement of the centre line of the plate for the first rolling pass. The inputs of the model are the external forces acting on the plate, the camber and the thickness profile of the incoming plate and the lateral asymmetries of the roll gap height. For brevity, the argument t for the time is omitted in this paper wherever confusion is ruled out.

2.1 Dynamical model of the plate motion

A free body diagram of the plate is shown in Fig. 2. The external forces F^- and F^+ (e. g. applied by edger rolls) are assumed to act on the plate upstream and

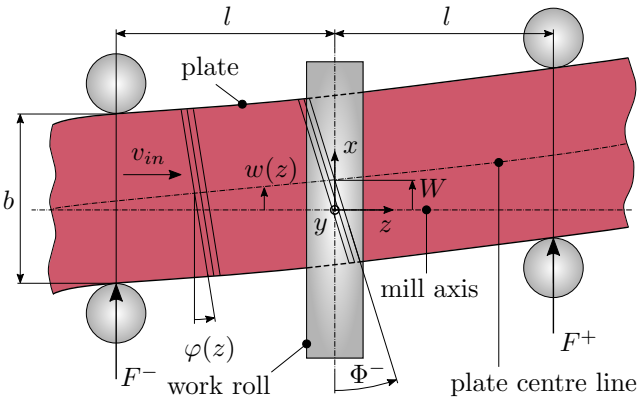

Fig. 2. Free body diagram of the plate (top view) (Ettl et al., 2018).

downstream, respectively, of the roll gap. Following Ettl et al. (2018), the dynamics of the lateral displacement W and the angular deflection Φ^- of the plate in the roll gap can be given in the time-free formulation

$$\begin{bmatrix}\Phi^{-\prime}\\ W'\end{bmatrix} = \begin{bmatrix}0 & 0\\ -1 & 0\end{bmatrix}\begin{bmatrix}\Phi^-\\ W\end{bmatrix} + \begin{bmatrix}-\frac{l}{E_l I_y^-} - \frac{lK_{\Sigma-}^-}{I_y^-} & \frac{lK_{\Sigma+}^-}{I_y^+}\\ \frac{1}{G_l A_s^-} & 0\end{bmatrix}\begin{bmatrix}F^-\\ F^+\end{bmatrix} + \\ + \begin{bmatrix}-1 & -\frac{K_h^-}{w_0} & -\frac{K_H^-}{w_0}\\ 0 & 0 & 0\end{bmatrix}\begin{bmatrix}\kappa^-\\ \Delta h\\ \Delta H\end{bmatrix} \tag{1}$$

with

$$(\cdot)' = \frac{\mathrm{d}}{\mathrm{d}z_{in}}(\cdot) = \frac{1}{v_{in}}\frac{\mathrm{d}}{\mathrm{d}t}(\cdot)\ . \tag{2}$$

The processed length z_{in} of the incoming plate serves as independent variable and v_{in} is the mean entry velocity of the plate. In (1), $\Phi^- = \varphi(0^-)$ and $W = w(0^-)$ are the angular deflection of the cross section and the lateral displacement of the plate centre line on the entry side $z = 0^-$ of the roll gap. The length l is defined in Fig. 2, E_l is the Young's modulus of the plate in the roll gap, I_y^- and I_y^+ the area moment of inertia of the plate cross section on the entry and exit side, respectively, $G_l A_s^-$ is the shear stiffness of the incoming plate cross section in the roll gap, w_0 is the width of the plate, and κ^- is the camber of the incoming plate. The sensitivities $K_{\Sigma-}^-$, $K_{\Sigma+}^-$, K_h^-, and K_H^- determine how the forces F^-, F^+, the thickness wedge Δh of the linearised thickness distribution

$$h\,(X, z) = \bar{h}\,(z) + \Delta h\,(z)\,X/w_0 \tag{3}$$

of the incoming plate, and the tilt of the roll gap ΔH, with

$$H\,(X) = \bar{H} + \Delta H X/w_0\ , \tag{4}$$

affect the input velocity profile and thus also the lateral movement of the plate. In (3) and (4), X is the Lagrangian coordinate, measured from the plate centre line with $X \in [-w_0/2, w_0/2]$. Moreover, $\bar{h}(z)$ and $\bar{H}$ donate the mean thickness of the incoming plate and the mean roll gap height, which corresponds to the mean output thickness of the plate.

As described by Ettl et al. (2018), (1) follows from Timoshenko's beam theory. However, in contrast to Ettl et al. (2018), three beams with different Young's moduli are assumed in this paper as shown in Fig. 3. In this way, it is considered that the area where plastification takes place differs from the areas outside the roll gap. The area left

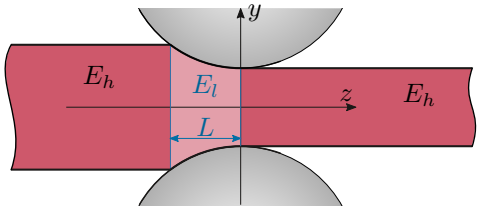

Fig. 3. Partitioning the plate into three Timoshenko beams with different Young's moduli (side view).

and right are modelled with a Young's modulus of E_h. The inner one is defined by the contact length L (Lenard, 2014) and a reduced Young's modulus of E_l to consider a softer area. Knowing that this does not cover plastic deformation in a physically correct way, the benefit of keeping a simple linear system structure is utilized at this point.

2.2 Camber evolution

Considering (Steinboeck et al., 2017), the curvature of the outgoing plate centre line (camber) is given by

$$\kappa^+ = \begin{bmatrix} -\frac{l\left(\frac{K^-_{\Sigma-}}{\lambda^2}-K^+_{\Sigma-}\right)}{I^-_y} & \frac{l\left(\frac{K^-_{\Sigma+}}{\lambda^2}-K^+_{\Sigma+}\right)}{I^+_y} \end{bmatrix} \begin{bmatrix} F^- \\ F^+ \end{bmatrix} + \\ + \begin{bmatrix} \frac{1}{\lambda^2}\left(\frac{K^-_h}{\lambda^2}-K^+_h\right) & \left(\frac{K^-_H}{\lambda^2}-K^+_H\right) \end{bmatrix} \begin{bmatrix} \kappa^- \\ \Delta h \\ \Delta H \end{bmatrix} . \quad (5)$$

Here, $\lambda = \bar{h}^-/\bar{H}$ is the ratio of the mean input and mean output thickness. The sensitivities $K^+_{\Sigma-}$, $K^+_{\Sigma+}$, K^+_h, and K^+_H determine how the input forces F^-, F^+, the thickness wedge Δh of the incoming plate, as well as the tilt of the roll gap ΔH affect the output velocity profile and therefore the resulting camber κ^+. The sensitivities satisfy (Steinboeck et al., 2017)

$$K^-_{\Sigma-} = K^+_{\Sigma-} \qquad 1 = \bar{h}\left(K^+_h - K^-_h\right)$$
$$K^-_{\Sigma+} = K^+_{\Sigma+} \qquad 1 = \bar{H}\left(K^-_H - K^+_H\right) .$$

3. CONTROL DESIGN

In addition to the reduction of the plate thickness, an important control task of the roughing mill is to minimize the lateral motion and the camber of the outgoing plate. From (Steinboeck et al., 2017), it is known that a cambered plate can pass the roll gap without lateral motion and thus both the lateral motion and the camber have to be controlled. In the considered rolling mill, only the inputs F^- and F^+ (defined by the edger positions) can be chosen and actively modified during the rolling pass. In this paper, a cascade control structure as depicted in Fig. 4 is proposed, with an admittance controller (AC) in the inner loop and an LQR in the outer loop.

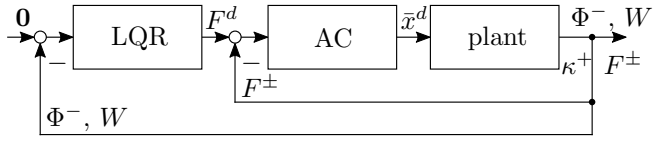

Fig. 4. Cascade control structure. Inner loop: admittance control (AC); Outer loop: LQR.

3.1 Admittance control

In the considered rolling mill, the edger rolls are positioned with an underlying position controller. In this way, the desired plate width $w_0 = x_1 - x_2 - 2R$, where x_1 and x_2 are the lateral positions of the edger rolls and R is their radius, can be reliably maintained and their mean position $\bar{x} = \frac{x_1+x_2}{2}$, which is relevant for F^- and F^+, can be easily adjusted. To exert the desired forces but also satisfy given constraints for $\bar{x}$ and $\dot{\bar{x}}$, an admittance control with nonlinear coefficients is designed. Assume that F^d is the desired lateral force of the edger rolls [1]. The admittance control law (Flixeder et al., 2017)

$$m^d\ddot{\bar{x}}^d + d^d\dot{\bar{x}}^d + k^d\bar{x}^d = \underbrace{k^P e + k^I \int e \mathrm{d}\tau}_{\tilde{F}} , \quad (6)$$

with the desired mass m^d, the damping coefficient d^d, the stiffness k^d, the control parameters k^P and k^I, and the force control error $e = F^d - F$, is used. The integral term on the right-hand side of (6) ensures a zero steady-state error. This controller requires the lateral force F to be measured, which can be easily done based on measured hydraulic pressures of the hydraulic edger positioning system.

In the steady state, (6) reduces to

$$k^d\bar{x}^d = \tilde{F} . \quad (7)$$

The stiffness coefficient k^d is chosen in the form

$$k^d = k^d_1 + k^d_2 , \quad k^d_1 = \frac{k_0}{e^{\frac{|\tilde{F}|}{k_0\bar{x}^d_{max}}}} , \quad k^d_2 = \frac{|\tilde{F}|}{\bar{x}^d_{max}} \quad (8)$$

to avoid that the absolute lateral displacement $|\bar{x}^d|$ exceeds the bound $\bar{x}^d_{max}$ in the stationary case. In (8), k_0 is a constant tuning parameter. Figure 5 shows the chosen stiffness and the resulting desired displacement $\bar{x}^d$. In an

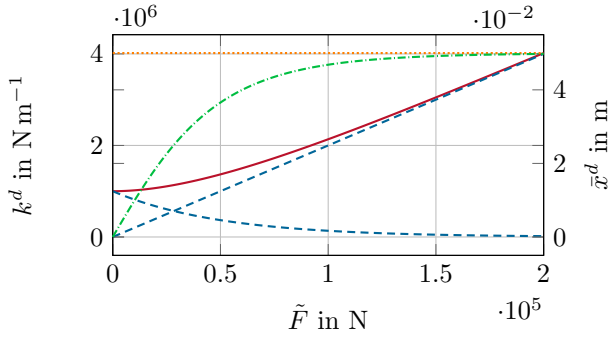

Fig. 5. Desired stiffness k^d (solid red), components of the stiffness k^d_1 and k^d_2 (dashed blue) and displacement $\bar{x}^d$ (dashdotted green) depending on $\tilde{F}$ for $\bar{x}^d_{max} = 50\,\mathrm{mm}$ (dotted orange) and $k_0 = 1\,\mathrm{MN\,m^{-1}}$.

analogous manner, a nonlinear damping coefficient

$$d^d = \frac{d_0}{e^{\frac{|\tilde{F}-k^d\bar{x}^d|}{d_0\dot{\bar{x}}^d_{max}}}} + \frac{\left|\tilde{F}-k^d\bar{x}^d\right|}{\dot{\bar{x}}^d_{max}} , \quad (9)$$

with a constant $d_0 > 0$, is used to avoid an absolute velocity $|\dot{\bar{x}}^d|$ larger than $\dot{\bar{x}}^d_{max}$. Note that (8) and (9)

[1] Note that in this paper desired values are denoted by the superscript d.

cannot strictly guarantee satisfaction of the constraints of $\bar{x}^d$. For instance, small values of d^d can lead to $\bar{x}^d > \bar{x}^d_{max}$ during transient phases. The desired mass is chosen as a constant $m^d = m_0$.

Because of the nonlinear stiffness (8), the steady-state error e is not necessarily zero and thus the integral term on the right hand side of (6) would grow without bounds. To avoid this undesirable behaviour, an anti-wind-up (AWP) strategy must be considered in the control design. It was found that simple box constraints of the value of the integral yield a satisfactory result. Moreover, this value is set to zero if the error e changes its sign.

3.2 LQR for the plate motion and camber

In this section, an LQR for the lateral motion and the camber of the outgoing plate is designed. It is assumed that the underlying admittance controller works sufficiently fast and thus the following control concept is developed for the model (1) and (5) with the control inputs F^- and F^+.

Because the shape of the plate is measured with cameras directly before and after the mill stand, the curvature κ^- is known (cf. Schausberger et al., 2015, 2016b). The roll gap height ΔH is defined by self-retaining electromechanical actuators. This implies that ΔH can only be adjusted before every rolling pass. During the pass, ΔH remains essentially constant, apart from the load-induced mill stretch. It is assumed that the roll gap height equals the thickness profile of the outgoing plate. Therefore, Δh is known for the subsequent rolling pass. Furthermore, the process variables ΔH and Δh can be treated as known disturbances in the controller design.

Assume that the design model (1) and (5) is discretized in the form

$$\boldsymbol{x}_{k+1} = \boldsymbol{\Phi}\boldsymbol{x}_k + \boldsymbol{\Gamma}_{u,\alpha}\boldsymbol{u}_k + \boldsymbol{\Gamma}_d\boldsymbol{d}_k \tag{10a}$$

$$y_k = \boldsymbol{D}_\alpha\boldsymbol{u}_k + \boldsymbol{H}\boldsymbol{d}_k\,, \quad \alpha \in \{b,i,o\}\,. \tag{10b}$$

Note that the index $k = 1,\dots,N$ refers to the nodes of a homogenous grid on the incoming plate with the spatial (independent) variable z_{in} and the grid spacing Δz_{in}. Thus, the length L_p of the incoming plate satisfies the relation $L_p = N\Delta z_{in}$. Moreover, Φ^- and W are summarized in the vector $\boldsymbol{x}_k$, F^- and F^+ in $\boldsymbol{u}_k$ and $\boldsymbol{d}_k$ combines the known inputs κ^-, Δh and ΔH. Because the camber of the outgoing plate (5) does not depend on the lateral position of the plate in the roll gap (1), (10b) does not depend on $\boldsymbol{x}_k$. In (10), three operational situations for a rolling mill with edger rolls on the entry and exit side are distinguished:

- edgers are active on both sides of the roll gap $\alpha = b$
- edgers are active on the entry side of the roll gap $\alpha = i$
- edgers are active on the exit side of the roll gap $\alpha = o$

During a rolling pass, the system switches between these three situations. Situation $\alpha = i$ is relevant for the thread-in phase. Then, situation $\alpha = b$ follows and finally situation $\alpha = o$ describes the thread-out phase. By analogy, model formulations for rolling mills that have edger rolls only at the entry or only at the exit side can be found. In these cases, however, there are also situations where the plate is clamped in the roll gap but not in contact with any edger rolls. During these phases, the motion and the camber of the plate cannot be controlled. In essence, three different controllers have to be designed for the situations $\alpha \in \{b,i,o\}$.

The control task is to regulate both the lateral plate motion W and the camber κ^+ of the outgoing plate to zero. The relative importance should be adjustable based on user-defined weighting parameters. Analogous to the classical LQR approach, the following optimization problem

$$\begin{aligned} &\underset{u_0,\dots u_N}{\arg\min}\; J\left(\boldsymbol{x}_0\right)\;, \\ J\left(\boldsymbol{x}_0\right) = &\sum_{k=0}^{N-1} \begin{bmatrix}\boldsymbol{x}_k^{\mathrm{T}} & \boldsymbol{u}_k^{\mathrm{T}} & y_k^{\mathrm{T}}\end{bmatrix} \begin{bmatrix}\boldsymbol{Q} & \boldsymbol{0} & \boldsymbol{0}\\ \boldsymbol{0} & \boldsymbol{R}_\alpha & \boldsymbol{0}\\ \boldsymbol{0} & \boldsymbol{0} & T\end{bmatrix} \begin{bmatrix}\boldsymbol{x}_k\\ \boldsymbol{u}_k\\ y_k\end{bmatrix} + \\ &\begin{bmatrix}\boldsymbol{x}_N^{\mathrm{T}} & \boldsymbol{u}_N^{\mathrm{T}} & y_N^{\mathrm{T}}\end{bmatrix} \begin{bmatrix}\boldsymbol{P}_N & \boldsymbol{0} & \boldsymbol{0}\\ \boldsymbol{0} & \boldsymbol{R}_\alpha & \boldsymbol{0}\\ \boldsymbol{0} & \boldsymbol{0} & T\end{bmatrix} \begin{bmatrix}\boldsymbol{x}_N\\ \boldsymbol{u}_N\\ y_N\end{bmatrix} \end{aligned} \tag{11}$$

has to be solved subject to system dynamics (10). In (11), $\boldsymbol{Q}$, $\boldsymbol{R}_\alpha$, $\boldsymbol{P}_N$ denote positive definite weighting matrices, and $T > 0$ is a weighting factor. Applying dynamic programming to (11) directly leads to the optimal control input

$$\boldsymbol{u}_k^* = \boldsymbol{K}_{x,\alpha}\boldsymbol{x}_k + \boldsymbol{K}_{d,\alpha}\boldsymbol{d}_k\,, \quad k = 0,\dots N-1 \tag{12}$$

with

$$\boldsymbol{K}_{x,\alpha} = -\left(\boldsymbol{R}_\alpha + \boldsymbol{D}_\alpha^{\mathrm{T}} T \boldsymbol{D}_\alpha + \boldsymbol{\Gamma}_{u,\alpha}^{\mathrm{T}}\boldsymbol{P}_N\boldsymbol{\Gamma}_{u,\alpha}\right)^{-1} \boldsymbol{\Gamma}_{u,\alpha}^{\mathrm{T}}\boldsymbol{P}_N\boldsymbol{\Phi} \tag{13a}$$

$$\boldsymbol{K}_{d,\alpha} = -\left(\boldsymbol{R}_\alpha + \boldsymbol{D}_\alpha^{\mathrm{T}} T \boldsymbol{D}_\alpha + \boldsymbol{\Gamma}_{u,\alpha}^{\mathrm{T}}\boldsymbol{P}_N\boldsymbol{\Gamma}_{u,\alpha}\right)^{-1} \left(\boldsymbol{D}_\alpha^{\mathrm{T}} T \boldsymbol{H} + \boldsymbol{\Gamma}_{u,\alpha}^{\mathrm{T}}\boldsymbol{P}_N\boldsymbol{\Gamma}_d\right) \tag{13b}$$

and

$$\boldsymbol{u}_N^* = -\left(\boldsymbol{R}_\alpha + \boldsymbol{D}_\alpha^{\mathrm{T}} T \boldsymbol{D}_\alpha\right)^{-1} \boldsymbol{D}_\alpha^{\mathrm{T}} T \boldsymbol{H}\boldsymbol{d}_N\,. \tag{14}$$

Moreover, $\boldsymbol{P}_k$ is iteratively found by the discrete Riccati equation

$$\begin{aligned} \boldsymbol{P}_k = \boldsymbol{Q} + \boldsymbol{\Phi}^{\mathrm{T}}\boldsymbol{P}_{k+1}\boldsymbol{\Phi} - \boldsymbol{\Phi}^{\mathrm{T}}\boldsymbol{P}_{k+1}^{\mathrm{T}}\boldsymbol{\Gamma}_{u,\alpha}\cdot \\ \left(\boldsymbol{R}_\alpha + \boldsymbol{D}_\alpha^{\mathrm{T}} T \boldsymbol{D}_\alpha + \boldsymbol{\Gamma}_{u,\alpha}^{\mathrm{T}}\boldsymbol{P}_{k+1}\boldsymbol{\Gamma}_{u,\alpha}\right)^{-\mathrm{T}} \boldsymbol{\Gamma}_{u,\alpha}^{\mathrm{T}}\boldsymbol{P}_{k+1}\boldsymbol{\Phi}\,, \end{aligned} \tag{15}$$

with $\boldsymbol{P}_N$ according to (11).

During the rolling pass, the control law (12), (13) switches from $\boldsymbol{K}_{x,i}$ and $\boldsymbol{K}_{d,i}$ to $\boldsymbol{K}_{x,b}$ and $\boldsymbol{K}_{d,b}$ and further to $\boldsymbol{K}_{x,o}$ and $\boldsymbol{K}_{d,o}$. Because the switching points depend only on z_{in} and each controller is used just once, the asymptotic stability of the individual control laws implies the asymptotic stability of the switched control law.

4. SIMULATION STUDIES

As can be seen in Fig. 4, the input to the plant, which corresponds to the output of the admittance controller, is the desired mean position $\bar{x}^d$ of the edger rolls. For the mathematical model (1), (5), the forces F^- and F^+ serve as control inputs. Thus, a model is required that links $\bar{x}^d$ with F^- and F^+, respectively. Using the three Timoshenko beams with different Young's moduli according

to Fig. 3, the forces F^- and F^+ can be calculated as a function of $\bar{x}$ in the form

$$F^{\pm} = V^{\pm}\bar{x} \ , \tag{16}$$

with

$$V^- = \frac{1}{\frac{(l-L)^3}{3E_h I_y^-} + \frac{L(L^2-3Ll+3l^2)}{3E_l I_y^-} + \frac{l-L}{G_h A_s^-} + \frac{L}{G_l A_s^-}} \tag{17a}$$

and

$$V^+ = \frac{1}{\frac{l^3}{3E_h I_y^+} + \frac{l}{G_h A_s^+}} \ . \tag{17b}$$

Moreover, the underlying position control loop can be well approximated, with an error of less than 2.5 %, by a lag element of second order

$$G_{PT2} = \frac{\hat{\bar{x}}}{\hat{\bar{x}}^d} = \frac{1}{T_e^2 s^2 + 2\xi T_e s + 1} \ , \tag{18}$$

where a hat ($\hat{\cdot}$) symbol refers to the corresponding Laplace transform.

The following simulations were conducted with the parameters given in Table 1 and a sampling time of $T_s = 1\,\mathrm{ms}$. The grid spacing Δz_{in} of the independent coordinate z_{in} thus satisfies the relation $\Delta z_{in,k} = v_{in,k} T_s$.

Table 1. Plant parameters.

name	value	unit	name	value	unit
l	3.3	m	k^P	0.25	1
L	0.14	m	k^I	1	m^{-1}
E_l	5e8	$\mathrm{N\,m}^{-2}$	k_0	1	$\mathrm{MN\,m}^{-1}$
E_h	1e11	$\mathrm{N\,m}^{-2}$	d_0	1	$\mathrm{N\,s\,m}^{-1}$
I_y^-	0.075	m^4	m_0	1	kg
I_y^+	0.063	m^4	$\bar{x}^d_{max}$	50	mm
G_l	$2 \cdot 10^8$	$\mathrm{N\,m}^{-2}$	$\dot{\bar{x}}^d_{max}$	0.4	$\mathrm{m\,s}^{-1}$
G_h	$4 \cdot 10^{10}$	$\mathrm{N\,m}^{-2}$	AWP lim.	500	kN
A_s^-	0.29	m^2	T_e	30	ms
A_s^+	0.25	m^2	ξ	3	1

4.1 Admittance control

In this section, the admittance control is investigated based on the plant model (16), (18). Consider a scenario where the plate is clamped by the edgers on the entry side and the work rolls in the roll gap. Assume that the plate does not move forward, i. e., $v_{in} = 0$. In this situation, a step of the desired asymmetric edger force is requested. The simulated response of the inner admittance control loop is shown in Fig. 6. The desired force level is not reached because of the constraint $\bar{x}^d \leq \bar{x}^d_{max}$. Fig. 6 also shows that neither $\bar{x}^d$ and $\dot{\bar{x}}^d$ nor $\bar{x}$ and $\dot{\bar{x}}$ violate their constraints.

4.2 LQR for the plate motion and camber

A simulation study of the whole cascade control structure according to Fig. 4 is performed. The LQR uses the parameters from Table 2. Figure 7 shows the corresponding simulation results [2]. It can be clearly seen that the system behaviour significantly changes at the switching points (between 2.8 m and 6.7 m both edgers are active). Moreover, the figure shows that the desired values $\Phi^- = 0$,

[2] Note that the x-axis of Fig. 7 has the dimension m because of the time-free formulation of (1) and (5).

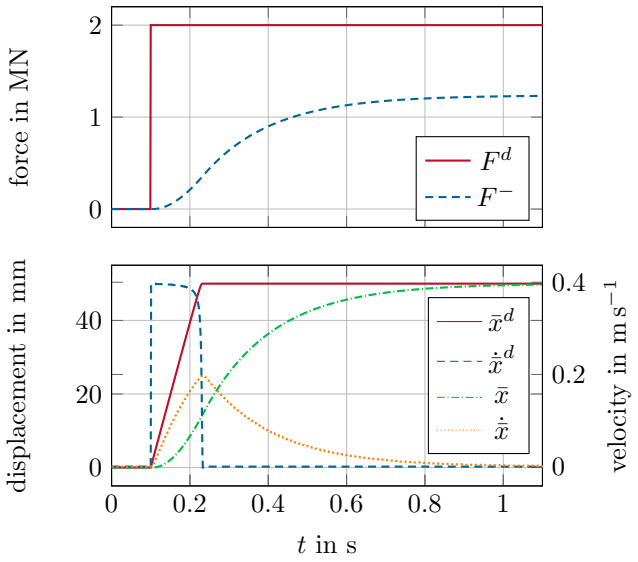

Fig. 6. Desired and actual force (upper graph) caused by a lateral displacement of the edger rolls (lower graph).

Table 2. Control parameters.

name	value	unit	name	value	unit
w_0	1.6	m	K_h^-	-4.02	m^{-1}
$\bar{h}$	220	mm	K_h^+	0.53	m^{-1}
$\bar{H}$	185	mm	K_H^-	4.75	m^{-1}
κ^-	1	km^{-1}	K_H^+	-0.66	m^{-1}
Δh	0.1	mm	$K_{\Sigma^-}^{\pm}$	2.12	$1/\mathrm{GN\,m}^2$
ΔH	0.25	mm	$K_{\Sigma^+}^{\pm}$	-2.12	$1/\mathrm{GN\,m}^2$
$\boldsymbol{R}_i$, $\boldsymbol{R}_o$	0	N^{-2}	$\boldsymbol{R}_b$	$\boldsymbol{I} \cdot 10^{-14}$	N^{-2}
$\boldsymbol{Q}$	$\boldsymbol{I} \cdot 0.1$	$\{\mathrm{rad}, \mathrm{m}\}^{-2}$	T	10^6	m^2

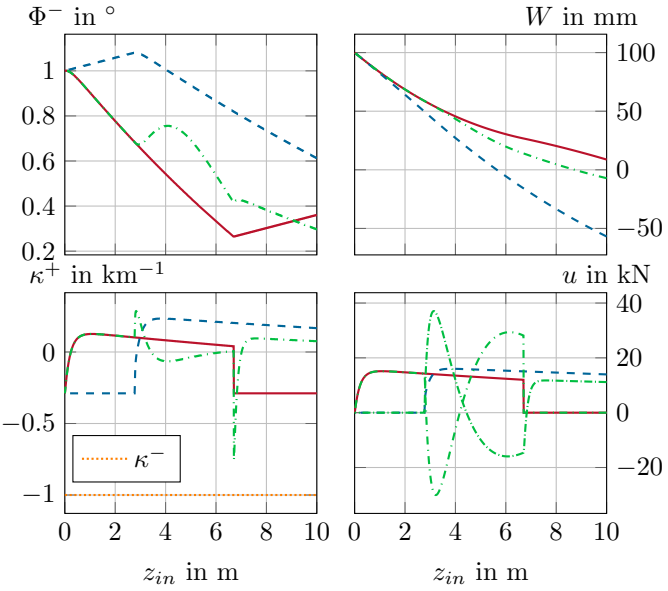

Fig. 7. Angular deflection (upper left graph), lateral displacement (upper right graph), camber of the outgoing plate (lower left graph), and control input (lower right graph) for the first rolling pass depicted for the case of edger rolls on the entry (solid red), exit (dashed blue) and both sides (dashdotted green) of the roll gap.

$W = 0$ and κ^+ are asymptotically reached if the controller is active.

From Fig. 7, it can be inferred that the control performance of a rolling mill with edgers at the entry and at the exit side is not significantly better compared to a rolling mill with edger rolls just on one side.

5. CONCLUSIONS

In heavy-plate rolling, there are many roughing mills where the roll gap height cannot be adjusted during the rolling pass. For such roughing mills, the possibility of using edger rolls to improve the lateral motion of the plate and to reduce its camber was examined.

The mathematical model of Ettl et al. (2018) was extended by partitioning the plate into three parts with different Young's moduli. With this approach, a softer area in the roll gap is considered by keeping the benefit of a simple linear model.

Because the extended model as well as the camber model of Steinboeck et al. (2017) have an external asymmetric force as their model input, an admittance controller was designed to provide those forces with the underlying position controller of the edger rolls. The proposed approach incorporates constraints on the lateral displacement of the edger rolls by nonlinear formulations of the stiffness and the damping coefficient in the target dynamics of the admittance controller.

In an outer control loop, an LQR controls the lateral displacement of the plate in the rolling gap and the camber of the outgoing plate. With user-defined weighting parameters the relative importance of these two system outputs can be considered in the controller design. Despite the switching behaviour of the plant, asymptotic stability of the system with the LQR is ensured, no matter if edgers are located on the entry, the exit, or on both sides of the roll gap.

Simulation studies showed that both the lateral displacement and the camber can be improved by the proposed cascade control concept. Moreover, the proposed concept can also be used for configurations with edgers at the entry or at the exit side of the roll gap. Configurations with edgers on both sides have the advantage that the controllability is ensured throughout the whole rolling pass.

The mathematical model as well as numerical values of this paper are based on real measurement data. Encouraged by the simulation results, an implementation and validation of the proposed control system at an industrial plant is planned for the near future.

ACKNOWLEDGEMENTS

The financial support by the Christian Doppler Research Association, the Austrian Federal Ministry for Digital and Economic Affairs, the National Foundation for Research, Technology and Development, and voestalpine Stahl GmbH is gratefully acknowledged.

REFERENCES

Cuzzola, F. and Dieta, N. (2003). Camber and wedge compensation in hot strip rolling. In *Proceedings of the IFAC Workshop on New Technologies for Automation of Metallurgical Industry*, 1–13. Shanghai, China.

Ettl, A., Prinz, K., Mueller, M., Steinboeck, A., and Kugi, A. (2018). Mathematical model and stability analysis of the lateral plate motion in a reversing rolling mill stand. *IFAC-PapersOnLine*, 51(2), 73–78.

Flixeder, S., Glück, T., and Kugi, A. (2017). Force-based cooperative handling and lay-up of deformable materials: Mechatronic design, modeling, and control of a demonstrator. *Mechatronics*, 47, 246–261.

Gates, D.J. and Tarnopolskaya, T. (2008). Linear theory for lateral displacements of a metal strip in a tandem cold-rolling mill with asymmetries. *Proceedings of the Institution of Mechanical Engineers, Part C: Journal of Mechanical Engineering Science*, 222(7), 1131–1148.

Ishikawa, T., Tozawa, Y., and Nishizawa, J. (1988). Fundamental study on snaking in strip rolling. *Transactions of the Iron and Steel Institute of Japan*, 28(6), 485–490.

Kainz, A., Pumhoessel, T., Kurz, M., Widder, M., Aigner, L., and Zeman, K. (2016). Prediction of camber formation, suppression and control of wedge-shaped hot rolled slabs by analytical concepts and finite elements. *IFAC-PapersOnLine*, 49(20), 238–243.

Kurz, M., Döll, R., Kainz, A., Pumhössel, T., and Zeman, K. (2015). Wedge and camber control. In *METEC and 2nd ESTAD*, 1–10. Düsseldorf, Germany.

Lee, J. and Choi, Y.J. (2014). Development of camber and steering control system in hot strip mill. In *Proceedings of the 2014 IEEE Emerging Technology and Factory Automation (ETFA)*, 1–4. Barcelona, Spain.

Lenard, J. (2014). *Primer on Flat Rolling*. Elsevier, Oxford, 2nd edition.

Schausberger, F., Steinboeck, A., and Kugi, A. (2015). Optimization-based estimator for the contour and movement of heavy plates in hot rolling. *Journal of Process Control*, 29, 23–32.

Schausberger, F., Steinboeck, A., and Kugi, A. (2016a). Optimization-based reduction of contour errors of heavy plates in hot rolling. *Journal of Process Control*, 47, 150–160.

Schausberger, F., Steinboeck, A., and Kugi, A. (2018). Feedback control of the contour shape in heavy-plate hot rolling. *IEEE Transactions on Control Systems Technology*, 26(3), 842–856.

Schausberger, F., Steinboeck, A., Kugi, A., Jochum, M., Wild, D., and Kiefer, T. (2016b). Vision-based material tracking in heavy-plate rolling. *IFAC-PapersOnLine*, 49(20), 108–113.

Steinboeck, A., Ettl, A., and Kugi, A. (2017). Dynamical models of the camber and the lateral position in flat rolling. *Applied Mechanics Reviews*, 69(4), 1–14.

Tanaka, Y., Omori, K., Miyake, T., Nishizaki, K., Inoue, M., and Tezuka, S. (1987). Camber control techniques in plate rolling. *Kawasaki Steel*, 16, 12–20.

Tarnopolskaya, T., Gates, D.J., de Hoog, F.R., and Yuen, W.Y.D. (2005). Instability in lateral dynamics of a metal strip in cold rolling. *ANZIAM Journal*, 46(0), 987–1000.

Yang, Y., Chen, C., Ho, C., Li, W., and Wu, J. (2008). Development of a camber measurement system in a hot rolling mill. In *2008 IEEE Industry Applications Society Annual Meeting*, 1–6. Edmonton, Canada.